RSC Advances

PAPER

View Article Online
View Journal | View Issue

Check for updates

Cite this: *RSC Adv.*, 2020, **10**, 26374

Structural control of magnetite nanoparticles for hyperthermia by modification with organic polymers: effect of molecular weight

Toshiki Miyazaki, *[a] Takayuki Tange,[a] Masakazu Kawashita [b] and Balachandran Jeyadevan [c]

Hyperthermia treatment using appropriate magnetic materials in an alternating magnetic field to generate heat has been recently proposed as a low-invasive cancer treatment method. Magnetite (Fe_3O_4) nanoparticles are expected to be an appropriate type of magnetic thermal seed for this purpose, and the addition of organic substances during the synthesis process has been studied for controlling particle size and improving biological functions. However, the role of the properties of the organic polymer chosen as the modifier in the physical properties of the thermal seed has not yet been comprehensively revealed. Therefore, this study clarifies these points in terms of the molecular weight and the charge of the functional groups of the added polymers. Excepting polyethyleneimine, the Fe_3O_4 crystallite size decreased with increasing polymer molecular weight. Neutral polymers did not suppress the Fe_3O_4 formation regardless of the difference in molecular weight, while suppression of the Fe_3O_4 formation was observed for low molecular weight anionic polymers and high molecular weight cationic polymers. Samples with a small amount of Fe_3O_4 or with crystallite size less than 10 nm induced low heat generation under an alternating magnetic field.

Received 12th May 2020
Accepted 8th July 2020

DOI: 10.1039/d0ra04220j

rsc.li/rsc-advances

Open Access Article. Published on 14 July 2020. Downloaded on 6/9/2026 9:23:18 AM.
This article is licensed under a Creative Commons Attribution-NonCommercial 3.0 Unported Licence.

1. Introduction

In cancer tissues, blood perfusion at 41 to 43 °C is typical, which is lower than in normal tissues.[1] Therefore, cancer cells can be killed at lower temperatures than would be necessary to kill normal cells. Based on this phenomenon, hyperthermia is attracting increasing attention as a novel cancer treatment to treat deep-seated cancers with minimal invasion.[2] Magnetic materials such as magnetite (Fe_3O_4) and maghemite (γ-Fe_2O_3) with appropriate physical properties achieve heat generation under an alternating magnetic field. When the size of Fe_3O_4 particles reaches the nanometer level, they become superparamagnetic, where Néel relaxation and Brownian relaxation are the primary heat generation mechanisms. Jeyadevan has theoretically studied the dependence of the specific absorption rate (SAR) upon particle size under a magnetic field strength and frequencies of 3.2 kA m^{-1} (40 Oe) and 600 kHz, respectively, and reported that SAR is maximized at a magnetite particle size around 12 nm.[3] However, improvement of cellular uptake of the Fe_3O_4 nanoparticles by surface modification is desired to enhance efficiency for the hyperthermia.[4]

Organic modification is a useful technique for enhancing the biological functionality of magnetic nanoparticles for hyperthermia such as the target drug delivery, gene therapy, sensing and so on.[5,6] In particular, the G250 antibody, capable of binding to the MN antigen in a tumor, has been conjugated with a magnetic liposome to impart a targeting function to the affected area. It was found that its uptake into the tumor increased six-fold compared with an un-conjugated magnetic liposome.[7] In addition, the molecular weight of the polymer modifier affects the viscosity, the aggregation state of the nanoparticles in liquid, and the immobilization density of their surfaces, besides changing biological functions. For example, modification of Fe_3O_4 nanoparticles with polyethylene glycol (PEG) of varying molecular weight exhibits a varying stability of the resulting conjugates in liquid.[8] It was also revealed that the cytotoxicity of Fe_3O_4 nanoparticles varies depending on the type of the polymer coating and the number of block copolymer units.[9,10]

Fe_3O_4 can be conventionally synthesized by an aqueous solution process.[11] If organic substances can be simultaneously incorporated during this process, a relatively simple one-pot manufacturing process can be established. For example, the size of spherical aggregates of Fe_3O_4 nanoparticles prepared by the hydrothermal method in the presence of polyacrylic acid (PAA) varies with the molecular weight of the PAA used during

[a]*Graduate School of Life Science and Systems Engineering, Kyushu Institute of Technology, 2-4 Hibikino, Wakamatsu-ku, Kitakyushu, Japan. E-mail: tmiya@life.kyutech.ac.jp*

[b]*Institute of Biomaterials and Bioengineering, Tokyo Medical and Dental University, Tokyo, Japan*

[c]*Department of Material Science, The University of Shiga Prefecture, Hikone, Shiga, Japan*

This journal is © The Royal Society of Chemistry 2020

Open Access Article. Published on 14 July 2020. Downloaded on 6/9/2026 9:23:18 AM.
This article is licensed under a Creative Commons Attribution-NonCommercial 3.0 Unported Licence.

the synthesis, where higher molecular weight corresponds to a smaller aggregate size.[12] Authors have found that the size and magnetic properties of the Fe_3O_4 nanoparticles vary depending on the functional groups of the added organic molecules added during the aqueous synthesis of Fe_3O_4, and that other types of iron hydroxide will form depending on the synthetic conditions.[13,14] However, the effects that the polymer molecular weight and functional groups have on the crystalline phase and the heat generation characteristics of the resulting conjugates have not been comprehensively investigated. Therefore, the purpose of this study was to clarify these points in terms of the molecular weight and the charge of the functional groups of the added polymers.

2. Materials and methods

2.1 Sample preparation

An aqueous co-precipitation method was used for the preparation of the samples. Specifically, $FeCl_2 \cdot 4H_2O$ (Wako Pure Chemical Industries Ltd., Osaka, Japan) and $FeCl_3 \cdot 6H_2O$ (Wako Pure Chemical Industries Ltd., Osaka, Japan) were dissolved in ultrapure water to prepare 50 mL of solution containing 2.5 mM Fe^{2+} and 4.9 mM Fe^{3+} while bubbling with N_2 gas. Separately, 100 mL of 2.0 mM polymer solution was prepared, using one of the four polymers PEG (molecular weight: 200, 600 and 6000, Wako Pure Chemical Industries Ltd., Osaka, Japan), PAA (molecular weight: 5000 and 25 000, Wako Pure Chemical Industries Ltd., Osaka, Japan), polystyrene sulfonate sodium salt (PSSS; molecular weight: 300 000 and 500 000, Alfa Aesar, Lancashire, UK), or polyethyleneimine (PEI; molecular weight: 600, 1800, and 10 000, Wako Pure Chemical Industries Ltd., Osaka, Japan). For sample nomenclature, the polymer abbreviation is followed by the polymer molecular weight used. For example, for the sample incorporating PEG with a molecular weight of 600, the solution containing polymer was mixed with the metallic ion solution at 75 °C while bubbling N_2 gas, and 1 M-NH_3 aqueous solution was added dropwise till a pH of 7 was achieved and stirred for 1 hour. Then it was packed in a cellulose Visking tube (Nihon Medical Science Inc., Osaka, Japan), immersed in ultrapure water, and dialyzed for 1 day to remove water-soluble salts in the solution. After 1 day of dialysis, the ultrapure water used for the dialysis was replaced and dialysis was performed again for an extra day. After the dialysis, the sample was dried at 60 °C for 3 days in an oven (NDO-700, Tokyo Rikakikai Co., Ltd., Tokyo, Japan) and then ground by a mortar.

2.2 Characterization

The crystalline structure of the obtained samples was characterized by powder X-ray diffraction (XRD; M03XHF22, Mac Science Co., Ltd., Yokohama, Japan). In XRD, a CuKα X-ray was used as a source; the voltage and of the current of the Cu tube were fixed at 40 kV and 30 mA, respectively; the step width was 0.020°; and the counting time was 1 s. The crystallite size of the obtained particles (t) was calculated by using Scherrer's equation:[15]

$$t = \frac{0.94\lambda}{B \cos \theta_B} \quad (1)$$

where λ, B, θ_B correspond to the wavelength (0.154 nm), half width of (311) diffraction of the magnetite, and the (311) diffraction angle, respectively, of the X-ray. The shape of the sample was examined by transmission electron microscopy (TEM; H-900NAR, Hitachi Ltd., Tokyo, Japan). The TEM samples were prepared by dispersing 1 mg of the sample in 5 mL of ultrapure water using an ultrasonic cleaner (2510J-MT, Emerson Japan Ltd., Kanagawa, Japan) for 10 min. The resulting suspension was dropped on an elastic carbon film suitable for TEM observation.

The surface zeta potential of the sample in ultrapure water was measured with a zeta potential analyzer (ELS-Z, Otsuka Electronics Co., Ltd., Osaka, Japan). A quartz cell was used for the measurement.

2.3 Measurement of Fe^{2+} concentration in aqueous solution in the presence of polymer

The change in Fe^{2+} concentration owing to the addition of the polymer was examined by an assay using 4,7-diphenyl-1,10-phenanthrolinedisulfonic acid, and disodium salt (Bathophenanthroline, Dojindo Laboratories, Kumamoto, Japan). The bathophenanthroline–Fe^{2+} complex exhibits visible-light absorption at 535 nm, while Fe^{3+} does not.[16] Herein, 10 mL of an aqueous solution containing 0.072 mM of iron chloride(II) and 0.020 mM of each polymer was prepared. Then, 0.0022 mmol of bathophenanthroline was added to the solution, and the mixture was stirred for 1 min to stabilize the coloring. The absorbance of the obtained solutions at 535 nm was subsequently measured by ultraviolet-visible spectroscopy (UV-Vis; V-630, JASCO Co., Tokyo, Japan).

2.4 Heat generation measurement

The temperature change the samples exhibited in an alternating magnetic field was measured, and the SAR of the samples was calculated. First, 100 mg of the sample was dispersed in 1 mL of 1 mass% agar boiling solution and naturally cooled. Sample concentration was higher than the previous study (4 mg mL^{-1}),[17] because magnetic field intensity was lower. The sample, now embedded in the agar phantom, was then placed in an alternating magnetic field generator consisting of a high frequency power supply (T162-5723A, Thamway Co. Ltd., Shizuoka, Japan), an impedance matching box (T020-5723C, Thamway Co. Ltd., Shizuoka, Japan), and a work coil. The alternating magnetic field application conditions were a frequency of 600 kHz, a magnetic field intensity of 3.2 kA m^{-1} (40 Oe), and an application time of 10 min. The temperature change of the sample was obtained using a fiber optic thermometer (OTG-MPK5, Opsens Inc., Québec, Canada) attached to a signal conditioner (TempSens, Opsens Inc., Québec, Canada). The SAR value was calculated from the temperature rise of the sample in an applied alternating magnetic field; using the relation

Open Access Article. Published on 14 July 2020. Downloaded on 6/9/2026 9:23:18 AM.
This article is licensed under a Creative Commons Attribution-NonCommercial 3.0 Unported Licence.

$$\mathrm{SAR}\left(\mathrm{W\ g^{-1}}\right) = \left(\sum_{\mathrm{i}} \frac{C_{\mathrm{i}} m_{\mathrm{i}}}{m_{\mathrm{Fe}}}\right) \times \frac{\Delta T}{\Delta t}, \quad (2)$$

where the subscript i is each substance (i = agar, Fe_3O_4), C_i is the specific heat capacity of each substance (J g^{-1} K^{-1}, C_{agar} = 4.18 J g^{-1} K^{-1}, $C_{Fe_3O_4}$ = 0.67 J g^{-1} K^{-1}), m_i is the mass of each substance (g), m_{Fe} is the mass of the Fe component (g), and ($\Delta T/\Delta t$) is the initial slope of temperature–time curve within 1 min after applying the magnetic field.

Magnetization behavior of the sample without polymer addition, PEG 200, PEG 6000 and PEI-added samples was measured by a superconducting quantum interference device (SQUID) (MPMS-XL7AC, Quantum Design Inc., San Diego, California, USA) in an applied DC magnetic field of ±2389 kA m^{-1} (30 kOe) at 27 °C.

Table 1 Crystallite size of Fe_3O_4 particles calculated from XRD patterns

Sample	Crystallite size/nm
None	21.3
PEG 200	15.5
PEG 600	13.8
PEG 6000	11.0
PSSS 300 000	18.3
PSSS 500 000	14.4
PAA 5000	11.4
PAA 25 000	8.5
PEI 600	19.3
PEI 1800	Not measured
PEI 10 000	Not measured

3. Results

Fig. 1 shows the XRD patterns of the samples prepared by addition of the polymers having various molecular weights. Although diffraction peaks from Fe_3O_4 (JCPDS # 19-0629) were detected from all samples, the peaks were notably weak for PAA 25 000, PEI 1800 and PEI 10 000. Additionally, the presence of a peak allocated to γ-FeOOH (JCPDS # 44-1415) was observed for PSSS 300 000 and PAA 5000 and α-FeOOH (JCPDS # 29-0713) for PEI 1800 and PEI 10 000. Table 1 summarizes crystallite sizes of the Fe_3O_4 particles determined from the XRD patterns. The crystallite sizes of all the samples were smaller than the sample without polymer addition. It tended to decrease with increase in molecular weight of the polymer.

Fig. 2 shows TEM micrographs of the samples. With the addition of PEG, spherical particles derived from Fe_3O_4 about 10–20 nm in size were observed. Although some spherical particles were observed with the addition of PSSS and PAA, many particles were needle-shaped with a major axis of 100–200 nm. The addition of PEI yielded a mix of spherical particles and needle-like particles derived from FeOOH in PEI 600 and PEI 1800, where the size of the spherical particles in the latter sample of several tens of nanometers was much larger than those in the other samples. In PEI 10 000, only needle-shaped particles were observed. Fig. 3 shows the Fe^{2+} concentration of the $FeCl_2$ solutions including polymers with various molecular weights. When PEG was added, the Fe^{2+} concentration was almost the same as that without polymer addition. With the addition of the other polymers, however, the Fe^{2+} concentration tended to decrease. In particular, PSSS addition significantly decreased the Fe^{2+} concentration in the solutions.

Fig. 4 shows the time-dependent temperature change of samples embedded in agar phantom under an alternating magnetic field. The temperature increase was about 23 °C without polymer addition, whereas that of the PEG 6000 sample was as high as about 38 °C. In addition, the temperature increase was 17 to 22 °C for the other PEG samples and the PSSS samples, and about 12 °C for PEI 600 and PAA 5000. Finally, the temperature increased by only about 2 °C for the remaining PEI samples and for PAA 25 000. Table 2 shows the SAR value of all samples calculated from the temperature–time curve, where a higher temperature increase corresponds to a higher SAR value.

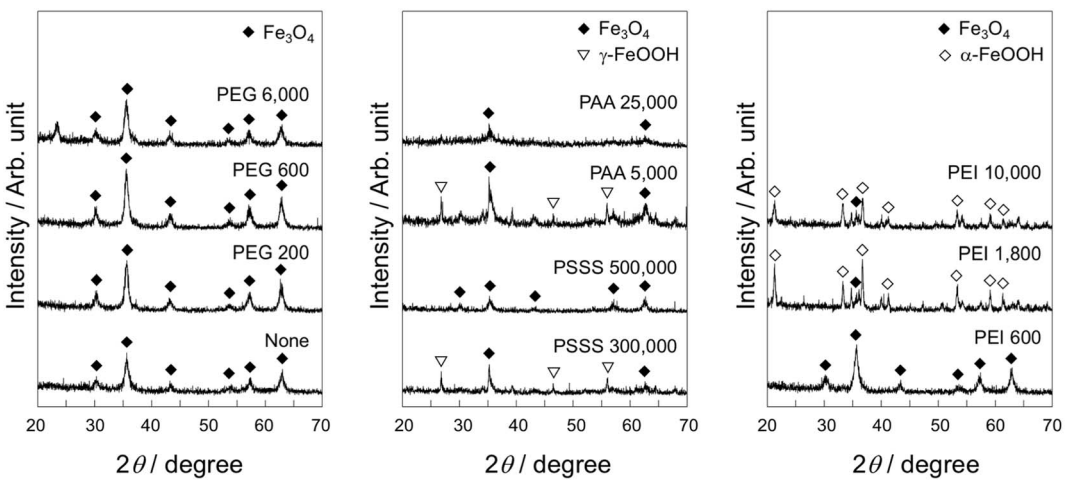

Fig. 1 XRD patterns of the samples prepared by addition of the polymers having various molecular weights.

 This journal is © The Royal Society of Chemistry 2020

Open Access Article. Published on 14 July 2020. Downloaded on 6/9/2026 9:23:18 AM.
This article is licensed under a Creative Commons Attribution-NonCommercial 3.0 Unported Licence.

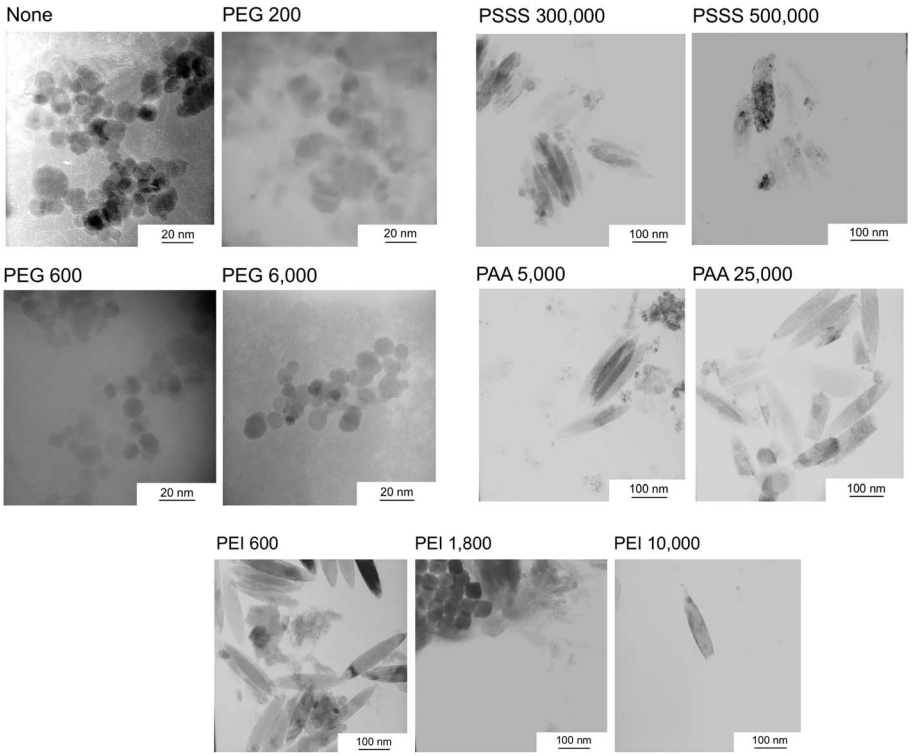

Fig. 2 TEM micrographs of the samples prepared by adding polymers of varying molecular weight.

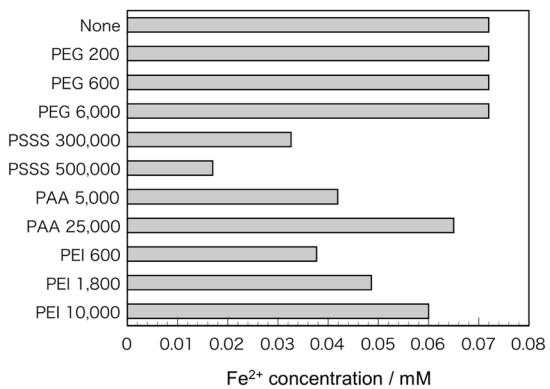

Fig. 3 Fe^{2+} concentration of $FeCl_2$ solutions including polymers of varying molecular weight.

Table 2 SAR calculated values of all samples

Sample	SAR (W g_{Fe}^{-1})
None	3.0
PEG 200	2.3
PEG 600	2.7
PEG 6000	4.5
PSSS 300 000	3.0
PSSS 500 000	2.2
PAA 5000	0.20
PAA 25 000	0.49
PEI 600	2.3
PEI 1800	0.29
PEI 10 000	0.49

Fig. 5 shows magnetization curves of the samples. Saturation magnetization increased in the order: PEI 10 000 (0.885 emu g^{-1}) < PEI 1800 (8.73 emu g^{-1}) < PEG 6000 (38.1 emu g^{-1}) < none (55.8 emu g^{-1}) < PEI 600 (55.9 emu g^{-1}) < PEG 200 (69.5 emu g^{-1}).

4. Discussion

It was found that the size and crystalline phase of the formed iron oxide greatly varied depending on the type and molecular weight of the added polymer. In the case of non-ionic PEG, Fe_3O_4 was formed regardless of its molecular weight, whereas the crystallite size of the formed nanoparticles decreased with increased PEG molecular weight. This size decrease can be attributed to the suppression of iron ion diffusion owing to the increased viscosity of the surrounding solution with increased molecular weight, with a consequent suppression of the crystal growth. However, PEG did not have a site capable of tight chelation with the iron ions, thus nucleation of Fe_3O_4 was not suppressed. This premise is supported by the results that the Fe^{2+} concentration in the PEG-containing solution decreased little compared with that of the solution without the polymer (Fig. 3).

When the anionic polymers PSSS and PAA were added, the crystal growth of Fe_3O_4 also tended to be suppressed. In the case

Open Access Article. Published on 14 July 2020. Downloaded on 6/9/2026 9:23:18 AM.
This article is licensed under a Creative Commons Attribution-NonCommercial 3.0 Unported Licence.

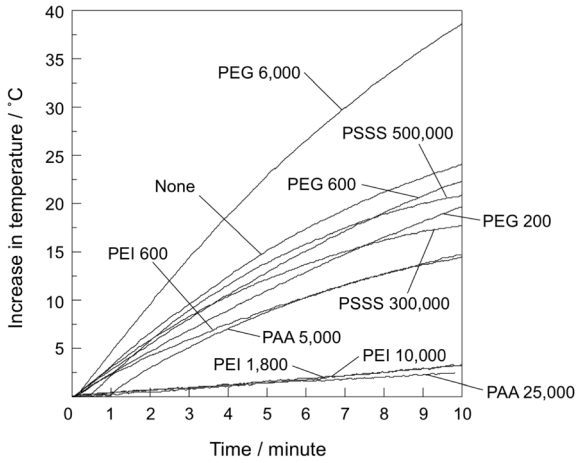

Fig. 4 Time-dependent temperature variation of the samples embedded in agar phantom under an alternating magnetic field.

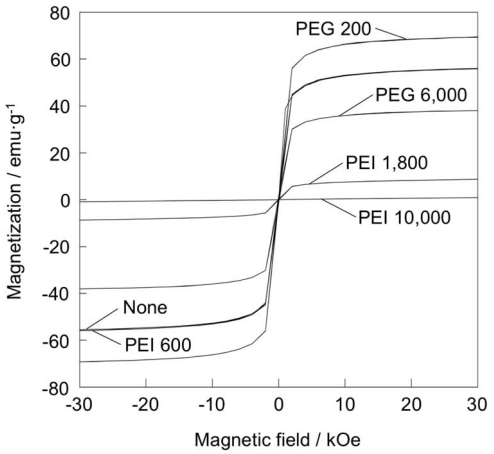

Fig. 5 Magnetization curves of the samples.

of PSSS, the crystallite size decreased with increased molecular weight, similar to the results of PEG. A previous study showed that PSSS with a molecular weight of 1 000 000 resulted in an average Fe_3O_4 particle size of 6.9 nm,[13] which is consistent with the trend in this study. This result is attributed to the chelating ability of PSSS with iron ions, supported by the results in Fig. 3. The crystal growth inhibition by PAA was stronger than PSSS. The stability constant of the $Fe(CH_3COO)^{2+}$ complex (3.38), comprising Fe^{3+} and a carboxyl group, is greater than that of the $FeSO_4^+$ complex (2.56), comprising Fe^{3+} and sulfonic group[18,19] In addition, the molecular weight of PAA is 1/10 or less that of PSSS. Therefore, it is considered that the polymer molecules can easily adsorb on the Fe_3O_4 nuclei owing to their high mobility and chelating ability. The addition of anionic polymers resulted in FeOOH as well as Fe_3O_4 (Fig. 1), indicating that the nucleation of Fe_3O_4 is also suppressed by the formation of the complex. Furthermore, the amount of Fe^{2+} required for Fe_3O_4 formation decreases owing to oxidation of the Fe^{2+}–polymer complex *via* dissolved O_2. A previous work reported no adverse effect on the crystalline structure of Fe_3O_4 synthesized by the reaction of $Fe(OH)_2$ and $NaNO_3$ in the presence of 0.0125 mM of PAA.[20] This absence of the effect observed in that previous work is attributed to the lower PAA concentration therein than used in the present study (2.0 mM).

A larger amount of FeOOH was formed by the addition of cationic PEI than the other three polymer types, and a remarkable inhibition of Fe_3O_4 nucleation was observed (Fig. 1). The amount of ionic functional groups in PEI is lower than that in most anionic polymers because of its lower molecular weight. Nevertheless, the decrease in Fe^{2+} with the presence of PEI was comparable to most anionic polymers (Fig. 3). In addition, PEI has an amino group in the main chain capable of chelating, indicating that PEI is less susceptible to its conformation. Therefore, PEI is considered to have a high chelating ability. The stability constant of the triethylenetetramine ($(CH_2NHCH_2CH_2NH_2)_2$) complex, possessing an atomic arrangement similar to PEI, against Fe^{3+} is reported to be around 8, which is greater than $FeSO_4^+$ and $Fe(CH_3COO)^{2+}$.[21]

In the present study, suppression of Fe_3O_4 formation tended to occur with anionic polymers of low molecular weight and cationic polymers of high molecular weight. This signifies that the relationship between the molecular weight of the added polymers and the crystalline phase of Fe_3O_4 varied depending on the charge of the polymer. The molecular weight,[21,22] conformation,[23] steric hindrance,[24] and side chain length[25] are the factors known to effect the stability constant of the polymer complex, meaning that the mineralization behavior in the presence of polymers is highly complicated. In this regard, further investigation using polymers having the same functional groups but different conformation is needed.

The crystalline structure of FeOOH as a byproduct varied depending on the added polymer. This can be attributed to the difference in the pH of the solution, as revealed in a previous investigation of the relationship between pH of the precursor solution containing Fe^{2+} and Cl^- and the crystalline phase of the produced FeOOH.[26] According to that work, γ-FeOOH is the primary crystalline phase for pH 4–7, a mixture of γ-FeOOH and α-FeOOH is present for higher pH, and primarily the α-FeOOH phase for pH > 12. The pH herein ranged from 3.5–5.8 for PAA and PSSS, and from 11.3–12.8 for PEI. Therefore, the present results are consistent with the earlier report.

Heat generation under an alternating magnetic field also varied greatly with the type and molecular weight of the added polymer (Fig. 4). Samples with a small amount of Fe_3O_4 or with crystallite sizes less than 10 nm tended to exhibit a low heat generation. Yanase *et al.* reported that heating at about 45 °C induces evolution of heat shock proteins that activate immune cells.[27] Considering that the initial temperature of all samples in this study was about 25 °C, the samples exhibiting a temperature increase of 20 °C or more are considered desirable for hyperthermia applications.

Heat generation of PEG 6000 was rather higher than that of the particles without polymer addition. The particle size of the former was smaller than the latter. Jeyadevan reports that the heat generation drastically decreases when particle size of Fe_3O_4 is less than 10 nm.[3] This is opposite tendency to the present results. Saturation magnetization of PEG 6000 was rather lower

 This journal is © The Royal Society of Chemistry 2020

Open Access Article. Published on 14 July 2020. Downloaded on 6/9/2026 9:23:18 AM.
This article is licensed under a Creative Commons Attribution-NonCommercial 3.0 Unported Licence.

than the sample without polymer addition (Fig. 5), meaning that magnetization ability is not likely a main governing factor. Zeta potential of the sample without polymer addition and PEG 6000 was 39.6 and −17.4 mV, respectively, while that of agarose is negative value.[28] Therefore, it is assumed that PEG 6000 well disperses in agar matrix by electrostatic repulsion and exhibited high Brownian relaxation. It is reported that the state of aggregation, apparent hydrodynamic size and resultant SAR vary depending on the type of polymer coated on the Fe_2O_3 nanoparticles, because the state of Brownian relaxation may be affected by the aggregation.[29]

Suto *et al.* investigated heat generation of Fe_3O_4 nanoparticles treated with a surfactant and embedded in polyvinyl alcohol hydrogels, and reported that SAR of the nanoparticles is 16.8 W $g_{Fe_3O_4}^{-1}$ at maximum.[30] The authors prepared Fe_3O_4 nanoparticles by NaOH treatment of chitosan hydrogels dispersed with Fe^{2+} and measured the heat generation at 24 kA m^{-1} (300 Oe) and 100 kHz.[31] Its effective specific absorption rate normalized by strength of the applied alternating magnetic field and frequency is 1.24×10^{-8} W g_{Fe}^{-1} Oe^{-2} Hz^{-1} at maximum, whereas that of PEG 6000 in this study is 4.7×10^{-9} W g_{Fe}^{-1} Oe^{-2} Hz^{-1}. These facts mean that SAR of the present samples is lower than the above described Fe_3O_4 nanoparticles. There is also possibility for difference in dispersion in hydrogel matrix. So further detailed investigation is necessary in the future.

Among the added polymers, PEI and PAA especially tended to suppress heat generation. This is attributed to the formation of non-magnetic FeOOH and the decrease in the size of Fe_3O_4. In the case of PEI 1800, heat generation was extremely small despite the fact that spherical particles of 50–60 nm size were observed by TEM (Fig. 2). This is supported by the result that its magnetization was also strongly suppressed (Fig. 5). Li *et al.* examined the particle size dependence of the heat generation characteristics of Fe_3O_4 nanoparticles, reporting that particles with an average size of 8 nm exhibited the highest heat generation.[32] They also reported that the heat generation tended to decrease with increasing particle size owing to loss of superparamagnetism. Additionally, amount of the formed Fe_3O_4 was small (Fig. 1). Therefore, the low heat generation ability of PEI 1800 can be explained by the above findings.

The crystallite sizes of both PEG 6000 and PAA 5000 were around 11 nm (Table 1), which is in the range of excellent heat generation reported by Jeyadevan.[3] Nevertheless, the temperature increase of the former was significantly higher than the latter (Fig. 4). Low heat generation of the latter would be attributed to reduced Fe_3O_4 content by formation of γ-FeOOH.

5. Conclusions

We investigated the effects that the molecular weight of various polymer additives in the aqueous synthesis of Fe_3O_4 nanoparticles had on their structure and their heat generation under an alternating magnetic field. The Fe_3O_4 crystallite size tended to decrease with increasing molecular weight. Furthermore, ionic polymers suppressed nucleation of Fe_3O_4, while the molecular weight dependence for suppression of Fe_3O_4 formation was different for anionic and cationic polymers. Heat generation was suppressed in the conditions where crystal growth of Fe_3O_4 was suppressed or where a large amount of the byproduct FeOOH was formed. Although the effect that the polymer structure has on the Fe^{2+}–polymer complex formation and on the resultant Fe_3O_4 nucleation is complicated and further investigation is needed in future, the findings in this study can provide fundamental guidelines for organic modification of magnetic nanoparticles for hyperthermia.

Conflicts of interest

The authors have no conflict of interest to declare.

Acknowledgements

We acknowledge Dr Masashi Tanaka and Prof. Masaki Mito, from Faculty of Engineering, Kyushu Institute of Technology, for SQUID measurement. We also thank Sara Maccagnano-Zacher, PhD, from Edanz Group (www.edanzediting.com/ac) for editing a draft of this manuscript.

References

1 C. W. Song, *Cancer Res.*, 1984, **44**, 4721S.
2 T. Kobayashi, *Biotechnol. J.*, 2011, **6**, 1342.
3 B. Jeyadevan, *J. Ceram. Soc. Jpn.*, 2010, **118**, 391.
4 A. K. Gupta and M. Gupta, *Biomaterials*, 2005, **26**, 1565–1573.
5 N. Zhu, H. Ji, P. Yu, J. Niu, M. U. Farooq, M. W. Akram, I. O. Udego, H. Li and X. Niu, *Nanomaterials*, 2018, **8**, 810.
6 S. O. Aisida, P. A. Akpa, I. Ahmad, T. Zhao, M. Maaza and F. I. Ezema, *Eur. Polym. J.*, 2020, **122**, 109371.
7 M. Shinkai, B. Le, H. Honda, K. Yoshikawa, K. Shimizu, S. Saga, T. Wakabayashi, J. Yoshida and T. Kobayashi, *Jpn. J. Cancer Res.*, 2001, **92**, 1138.
8 J. D. Goff, P. P. Huffstetler, W. C. Miles, N. Pothayee, C. M. Reinholz, S. Ball, R. M. Davis and J. S. Riffle, *Chem. Mater.*, 2009, **21**, 4784.
9 U. O. Häfeli, J. S. Riffle, L. Harris-Shekhawat, A. Carmichael-Baranauskas, F. Mark, J. P. Dailey and D. Bardenstein, *Mol. Pharm.*, 2009, **6**, 1417.
10 V. Zavisova, M. Koneracka, A. Gabelova, B. Svitkova, M. Ursinyova, M. Kubovcikova, I. Antal, I. Khmara, A. Jurikova, M. Molcan, M. Ognjanović, B. Antić and P. Kopcansky, *J. Magn. Magn. Mater.*, 2019, **472**, 66.
11 K. Petcharoena and A. Sirivat, *Mater. Sci. Eng., B*, 2012, **177**, 421–427.
12 Y. Song, Y. Li, Z. Teng, Y. Huang, X. Chen and Q. Wang, *ACS Omega*, 2018, **3**, 17904.
13 Y. Kuwahara, T. Miyazaki, Y. Shirosaki and M. Kawashita, *RSC Adv.*, 2014, **4**, 23359.
14 Y. Kuwahara, T. Miyazaki, Y. Shirosaki, G. Liu and M. Kawashita, *Ceram. Int.*, 2016, **42**, 6000.
15 B. D. Cullity and S. R. Stock, *Elements of X-ray diffraction*, Prentice Hall, New Jersey, 3rd edn, 2001.
16 L. Montás-Ramírez, N. Claassen and A. M. Moawad, *J. Plant Nutr.*, 2003, **26**, 2023.

Open Access Article. Published on 14 July 2020. Downloaded on 6/9/2026 9:23:18 AM.
This article is licensed under a Creative Commons Attribution-NonCommercial 3.0 Unported Licence.

17 T. Miyazaki, A. Miyaoka, E. Ishida, Z. Li, M. Kawashita and M. Hiraoka, *Mater. Sci. Eng., C*, 2012, **32**, 692.
18 A. E. Martell and R. M. Smith, *Critical Stability Constants*, Plenum Press, New York, 1975.
19 Y. Kanroji, *Yakugaku Zasshi*, 1963, **83**, 424 (in Japanese).
20 E. Baumgartner and M. Mijalchik, *J. Colloid Interface Sci.*, 1991, **145**, 274.
21 *Stability Constants of Metal-ion Complexes*, ed. L. G. Sillén and A. E. Martell, The Chemical Society, London, 1964.
22 O. D. Kochkodan, V. M. Kochkodan and V. K. Sharma, *J. Environ. Sci. Health, Part A: Toxic/Hazard. Subst. Environ. Eng.*, 2018, **53**, 33.
23 H. P. Gregor, L. B. Luttinger and E. M. Loebl, *J. Phys. Chem.*, 1955, **59**, 34.
24 M. Feng, L. van der Does and A. Bantjes, *J. Appl. Polym. Sci.*, 1995, **56**, 1231.
25 A. Winston, in *Bioactive Polymeric Systems: An Overview*, ed. C. G. Gebelein and C. E. Carraher Jr, Plenum Press, New York, 1985, pp. 621–649.
26 H. Tamura, K. Takahashi and M. Nagayama, *Bull. Fac. Eng., Hokkaido Univ.*, 1977, **85**, 93 (in Japanese).
27 M. Yanase, M. Shinkai, H. Honda, T. Wakabayashi, J. Yoshida and T. Kobayashi, *Jpn. J. Cancer Res.*, 1998, **89**, 775.
28 F. G. Adivi, P. Hashemi and A. D. Tehrani, *Polym. Bull.*, 2019, **76**, 1239.
29 M. Babič, D. Horák, M. Molčan and M. Timko, *J. Phys. D: Appl. Phys.*, 2017, **50**, 345002.
30 M. Suto, Y. Hirota, H. Mamiya, A. Fujita, R. Kasuya, K. Tohji and B. Jeyadevan, *J. Magn. Magn. Mater.*, 2009, **321**, 1493.
31 T. Miyazaki, A. Iwanaga, Y. Shirosaki and M. Kawashita, *Colloids Surf., B*, 2019, **179**, 334.
32 Z. Li, M. Kawashita, N. Araki, M. Mitsumori, M. Hiraoka and M. Doi, *Mater. Sci. Eng., C*, 2010, **30**, 990.

This journal is © The Royal Society of Chemistry 2020